Articles in PresS. Am J Physiol Heart Circ Physiol (March 24, 2006). doi:10.1152/ajpheart.00084.2006

# Effect of Simulated $I_{to}$ on Guinea Pig and Canine Ventricular Action Potential Morphology

Min Dong[1], Xiaoyin Sun[1], Astrid A Prinz[2], Hong-Sheng Wang[1]

[1]Department of Pharmacology and Cell Biophysics, University of Cincinnati College of Medicine, Cincinnati, OH 45267
[2]Department of Biology, Emory University, Atlanta, GA 30322

**Running Head:** Role of $I_{to}$ in Shaping Cardiac Action Potential

**Contact Information:** Hong-Sheng Wang, Department of Pharmacology and Cell Biophysics, University of Cincinnati College of Medicine, Cincinnati, Ohio 45267-0575
Phone: (513) 558-2379
Email: wanghs@uc.edu

Copyright Information

Copyright © 2006 by the American Physiological Society.

## Abstract

The transient outward current ($I_{to}$) is a major repolarizing current in the heart. Marked reduction of $I_{to}$ density occurs in heart failure, and is accompanied by significant action potential duration (APD) prolongation. To understand the species-dependent role of $I_{to}$ in regulating the ventricular action potential morphology and duration, we introduced simulated $I_{to}$ conductance in guinea pig and canine endocardial ventricular myocytes using the dynamic clamp technique and perforated patch clamp recordings. The effects of simulated $I_{to}$ in both types of cells were complex and bi-phasic, separated by a clear density threshold of about 40 pA/pF. Below this threshold, simulated $I_{to}$ resulted in a distinct phase 1 notch, and had little effect on or moderately prolonged the APD. $I_{to}$ above the threshold resulted in all-or-none repolarization and precipitously reduced the APD. Qualitatively, these results agreed with our previous studies in canine ventricular cells using whole-cell recordings. We conclude that, contrary to previous gene transfer studies involving the Kv4.3 current, the response of guinea pig ventricular myocytes to a fully-inactivating $I_{to}$ is similar to that of canine ventricular cells, and that in animals such as dogs that have a broad cardiac action potential, $I_{to}$ does not play a major role in setting the APD.


**Key Words:** dynamic clamp; transient outward current; ventricular myocytes; action potential



Copyright Information

## Introduction

The transient outward potassium current, or $I_{to}$, is a key repolarizing current in the heart. The influence of $I_{to}$ on cardiac action potential waveform and duration is remarkably dependent on species. In smaller animals such as mouse and rat, $I_{to}$ is the dominant repolarizing current, and the high levels of $I_{to}$ in these animals are mostly responsible for the short duration and triangular shape of the action potential (2,23,27). In large animals including humans, it is well known that $I_{to}$ is responsible for phase-1 repolarization of the action potential. However, the influence of $I_{to}$ on action potential duration (APD) is less clear. The use of a pharmacological approach in studying the problem is hampered by the lack of specific $I_{to}$ blockers. An alternative method, mathematical simulation, has produced somewhat inconsistent results, predicting that physiological levels of $I_{to}$ do not affect (5,34) or significantly prolong (11) the APD.

In an earlier study, we used the dynamic clamp technique to study the role of $I_{to}$ in shaping the action potential in canine left ventricle (27). The dynamic clamp combines computer simulation with experimental electrophysiology, and allows the introduction of programmable artificial conductances in living cells. We have shown that $I_{to}$, while being a key regulator of phase 1 repolarization, does not play a major role in regulating the APD over a wide current density range that encompasses the $I_{to}$ densities found in canine ventricular cells. At densities above a threshold (a value that is much higher than the physiological $I_{to}$ levels in canine ventricle), $I_{to}$ precipitously shortens the APD and results in all-or-none repolarization.

Our study also suggests that the difference in $I_{to}$'s effect on action potential morphology in small and large animals is due, at least partially, to the dramatic difference


Copyright Information

in $I_{to}$ density in these species (27). Interestingly, our results in canine ventricular cells contrast with previous studies in guinea pig ventricular myocytes (9,10). Guinea pigs are unusual in their lack of native $I_{to}$ in the heart (4,36), and in the studies by Hoppe et al, exogenous Kv4.3 current was introduced into guinea pig ventricular myocytes by either gene transfer or cell fusion techniques. Introduction of such an $I_{to}$-type current did not generate a phase 1 notch, but progressively suppressed the action potential plateau and shortened the APD over the same $I_{to}$ density range as what we have tested in canine ventricular cells. The strikingly different observations in canine and guinea pig ventricular cells raise the possibility that guinea pig cells are unique not only in their total lack of native $I_{to}$, but also in their electrophysiological response to an exogenous $I_{to}$. It is plausible that due to the peculiar electrophysiological profile of the guinea pig cells, the threshold for all-or-none repolarization in these cells is much lower. As a result, the presence of even low to moderate densities of $I_{to}$ suppresses the development of the action potential plateau and shortens the APD. To test this possibility, and to further understand the species-dependent role of $I_{to}$ in shaping the action potential, in this paper we performed dynamic clamp simulations of $I_{to}$ in guinea pig ventricular cells.

A notable limitation of our earlier study (27) is the use of the whole-cell patch clamp and intracellular $Ca^{2+}$ buffer, which can alter $Ca^{2+}$ intracellular handling and affect the action potential properties. In the present study, to preserve physiological intracellular $Ca^{2+}$ handling we used the perforated patch clamp for all action potential recordings. We carried out simulation studies of $I_{to}$ in canine endocardial myocytes using the perforated patch clamp to verify our earlier results, and to allow side-by-side comparison of canine and guinea pig ventricular cells.


Copyright Information

## Materials and Methods

### Preparation of isolated guinea pig and canine ventricular myocytes

Handling and usage of animals were in accordance with protocols approved by the University of Cincinnati Institutional Animal Care and Use Committee. Adult guinea pigs weighing 200-250mg of either sex were anaesthetized by intraperitioneal injection of sodium pentobarbital (150mg $kg^{-1}$ body weight). Hearts were then quickly excised and mounted on a Langendorff perfusion apparatus, and perfused with oxygenated $Ca^{2+}$-free and then $Ca^{2+}$-containing (1.5 mM) solution for 5 minutes each. The perfusion solution contained (in mM): NaCl 112, KCl 5.4, $NaH_2PO_4$ 1.7, $MgCl_2$ 1.63, $NaHCO_3$ 4.2, HEPES 20, Glucose 5.4 and Taurine 10 (pH = 7.6). This was followed by perfusion with the same solution containing zero $Ca^{2+}$ and 85 unit $ml^{-1}$ collagenase (type II, Worthington) at 37°C until the hearts became flaccid. The ventricles were removed and minced and pipette-triturated in oxygenated KB solution containing (in mM): KCl 83, $K_2HPO_4$ 30, $MgSO_4$ 5, Na-pyruvate 5, ß-OH butyric acid (sodium salt) 5, taurine 20, creatine 5, glucose 10, EGTA 0.5, HEPES 5, and $Na_2ATP$ 5 (pH = 7.4). Cells were stored in the KB solution at room temperature and used on the day of isolation.

Adult dogs of either sex were euthanized with an intravenous injection of sodium pentobarbital at a concentration of 80 mg $kg^{-1}$ body weight. The heart was excised and a wedge-shaped left ventricular free wall was dissected. The tissue was then cannulated via a descending branch of the left circumflex artery and perfused with an oxygenated solution containing (in mM): NaCl 135, KCl 5.4, $MgCl_2$ 1.0, $NaH_2PO_4$ 0.33, HEPES 10, and glucose 10 (pH = 7.4), and then with the same solution containing 140 unit $ml^{-1}$ collagenase (type II, Worthington), 25 μM leupeptin and 0.32 unit $ml^{-1}$ protease (type


Copyright Information

XIV, Sigma) at 37°C for 10-15 min. Thin slices of tissue (<2 mm in thickness) were then removed from the endocardial surface, minced and gently shaked in the presence of a lower concentration of collagenase (110 unit $ml^{-1}$). Isolated myocytes were harvested and stored in a standard Tyrode solution containing 0.1 mM $Ca^{2+}$ at room temperature or 4°C, for recordings on the same day or the following day.

**Electrophysiological recordings**

Isolated cells were perfused with Tyrode's solution containing (in mM): NaCl 140, KCl 5.4, $MgCl_2$ 1, $CaCl_2$ 1.8, HEPES 5, and glucose 10 (pH = 7.4). Perforated patch-clamp recordings were used for action potential recordings and the dynamic clamp studies. Glass pipettes were back-filled with a pipette solution containing (in mM): K-aspartate 110, KCl 20, NaCl 8, HEPES 10, $MgCl_2$ 2.5, $CaCl_2$ 0.1, and 240 mg/ml amphotericin B (pH adjusted to 7.2 with KOH), and have a resistance of 1.5 – 2.0 MΩ. Cells were studied once stable series resistance <7 MΩ was achieved; cells with unstable or a higher series resistance were rejected. Series resistance was fully compensated under current clamp. For $K^+$ current recordings, whole-cell patch clamp recordings were used. 0.2 mM $CdCl_2$ was added to the external solution to block the $Ca^{2+}$ current. Pipette solution contained (in mM): K-aspartate 110, KCl 20, EGTA 10, HEPES 10, $MgCl_2$ 2.5, NaCl 4, $CaCl_2$ 1, $Na_2$-ATP 2, and Na-GTP 0.1 (pH adjusted to 7.2 with KOH). Both perforated and whole-cell patch clamp recordings were performed with an Axopatch-1B amplifier. Data were collected using PCLAMP9 software through an Axon Digidata 1322A data acquisition system. All experiments were performed at 34°C with the


Copyright Information

exception of $I_K$ recordings, which were carried out at room temperature (24°C). All chemical and drugs were from Sigma unless otherwise stated.

**Implementation of the dynamic clamp**

Dynamic clamp experiments were performed as previously described (27). A modified version of the Windows-based DynClamp software was used in the dynamic clamp studies (21). Voltage sampling of the dynamic clamp software and output of the current injection command were through an Axon Digidata 2100 board.

$I_{to}$ was defined as a rapidly and fully inactivating outward current, and was formulated based on our previous canine epicardial $I_{to}$ model (27). Modifications were made to account for shifts of the voltage-dependence of $I_{to}$ gating properties by external $Cd^{2+}$ (26,33). The $I_{to}$ conductance was given by:

$$I_{to} = g_{to} m h R (V_m - E_K) \quad (1)$$

$$R = \exp(V_m / 300) \quad (2)$$

$$\alpha_m = \frac{4}{1 + \exp((V_m - 25)/-20)} \quad (3)$$

$$\beta_m = \frac{3.5}{1 + \exp((V_m + 110)/29.5)} \quad (4)$$

$$m_\infty = \frac{1}{1 + \exp((V_m + 13.9)/-8)} \quad (5)$$

$$\alpha_h = \frac{0.016}{1 + \exp((V_m + 59)/5.5)} \quad (6)$$

$$\beta_h = \frac{0.11}{1 + \exp((V_m + 27)/-6.5)} \quad (7)$$


Copyright Information

$$h_{\infty} = \frac{1}{1 + \exp((V_m + 50.3)/3.9)} \quad (8)$$

Figure 1 shows the waveform, true peak conductance-voltage relationship, and voltage-dependencies of steady-state and time constants of the m and h gates of the model $I_{to}$. $E_K$, the reversal potential for $K^+$, was set to –85 mV. The electrode junction potential was 12 mV, and was corrected on-line in the computation. Action potentials were triggered with just-threshold 2 ms current steps and recorded at steady-state. Action potentials were re-controlled after each simulation. Because $g_{to}$ in equation 1 does not equal the true simulated $I_{to}$ conductance, the true peak current density in response to a depolarizing step from –80 mV to +40 mV is given to indicate the amplitude of the simulated $I_{to}$ unless otherwise stated.

**Data analysis**

Group data are presented as means ± S.E.M. Statistical tests of the effects of the dynamic clamp simulation were performed using paired, two-tail Student's t-tests. Other statistical tests used unpaired Student's t-tests. A *t* value giving $P < 0.01$ was considered as significant.


Copyright Information

## Results

### Electrophysiological properties of guinea pig ventricular myocytes

We first examined the action potentials of guinea pig ventricular cells using the perforated current clamp. Figure 2A shows representative action potentials triggered at 1 and 3 Hz. Notably, the action potentials lacked phase 1 repolarization, and had a waveform similar to that in canine endocardial ventricular cells (27). The average $APD_{90}$ at 1 Hz was 196.4 ± 12.1 ms (n = 18), and was abbreviated to 137.4 ± 9.9 ms at 3 Hz (n = 6). Consistent with their lack of phase 1 notch, whole-cell voltage clamp recordings showed no detectable $I_{to}$ in guinea pig ventricular cells (Fig 2B). By comparison, in response to the same voltage clamp protocol and under the same recording conditions, a robust $I_{to}$ was evident in canine epicardial cells (Fig 2B, inset). Repolarizing currents in guinea pig ventricular cells were dominated by a large delayed rectifier, or $I_K$ (Fig 2C).

### Dynamic clamp simulation of $I_{to}$ in guinea pig ventricular cells

To understand the role of $I_{to}$ in shaping the action potential, we introduced a simulated canine ventricular $I_{to}$ conductance in guinea pig ventricular cells using the dynamic clamp. Action potentials were triggered at 1 Hz and recorded at steady-state. Simulation of a typical canine epicardial-sized $I_{to}$ in guinea pig ventricular cells produced a distinct phase 1 notch and a “spike-and-dome” action potential configuration, but did not significantly affect the APD (Fig 3A). The use of the perforated patch clamp presented a challenge for the implementation of the dynamic clamp. We only studied cells with stable series resistance <7 MΩ, which was carefully monitored and fully


Copyright Information

compensated. The dynamic clamp output (Fig 3A, inset) and the voltage traces were without oscillation or distortion.

We examined the density-dependent effect of simulated $I_{to}$ on the action potential. Over a wide density range, simulated $I_{to}$ produced a distinct phase 1 notch and a spike-and-dome action potential waveform (Fig 3B). Low densities of $I_{to}$ did not significantly affect the APD (Fig 3B, left); as the $I_{to}$ density was further increased, the APD was moderately prolonged (Fig 3B, left, bold line) before reaching a threshold at which point the action potential alternated between one with a deep notch and a markedly prolonged APD and all-or-none repolarization (Fig 3B, right, bold lines). Any simulated $I_{to}$ larger than the threshold produced a brief, spike-like action potential (Fig 3B, right). Figure 3C shows the $I_{to}$ density-$APD_{90}$ relationships for the 18 guinea pig cells we studied, and the average data are shown in figure 3D. When the simulated $I_{to}$ was 21.9 ± 5.3 and 27.3 ± 6.2 pA/pF, $APD_{90}$ was not significantly changed (0.98 ± 0.05 and 1.00 ± 0.04 times the control value, n = 16 and 14, respectively; $P > 0.2$). Prolongation of APD was observed with 33.2 ± 5.5 and 39.4 ± 5.6 pA/pF of $I_{to}$, which resulted in $APD_{90}$ values of 1.06 ± 0.05 and 1.18 ± 0.06 times control, respectively (n = 18 for both, $P < 0.01$). Larger $I_{to}$ produced dramatic shortening of the APD: $APD_{90}$ ratio was reduced to 0.21 ± 0.11 with a simulated $I_{to}$ of 43.9 ± 5.9 pA/pF (n = 11, $P < 0.001$).

**Dynamic clamp simulation of $I_{to}$ in canine endocardial myocytes**

To allow comparison between guinea pig and canine ventricular cells, and to verify our earlier $I_{to}$ simulation results in canine ventricular cells, we performed dynamic clamp simulations of $I_{to}$ in canine endocardial cells using the perforated patch clamp. The


Copyright Information

overall effect of simulated $I_{to}$ on canine endocardial APD was similar to that in guinea pig cells (Figs 3 & 4), and qualitatively similar to our earlier results (27). Low levels of $I_{to}$ had little effect on the APD; further increases in $I_{to}$ density progressively and moderately prolonged the APD before collapsing the plateau and markedly shortened the APD (Fig 4). When the simulated $I_{to}$ was 22.8 ± 1.7 and 28.6 ± 2.0 pA/pF, the $APD_{90}$ ratios over control were 1.02 ± 0.01 and 1.05 ± 0.01, respectively (n = 8 and 5, $P > 0.02$ and $< 0.01$, respectively). $APD_{90}$ was further prolonged to 1.12 ± 0.02 and 1.19 ± 0.03 times control with a simulated $I_{to}$ of 33.2 ± 1.5 and 40.2 ± 1.9 pA/pF, but was shortened to 19 ± 0.3% of control with an $I_{to}$ of 44 ± 2 pA/pF (n = 7, $P < 0.01$ for all groups).

**Effect of model formulation and stimulation rate**

Compared to pure mathematical modeling, the dynamic clamp has the advantage of working with real, living cells, but still involves simulation of artificial conductances. To determine whether our $I_{to}$ simulation results are unique to the particular formulations of our canine epicardial $I_{to}$ model or instead represent a true $I_{to}$ effect, we performed simulations of an atrial $I_{to}$ model (24) in guinea pig ventricular cells, and compared its effects with those of our ventricular $I_{to}$ model. An example of such simulation is shown in figure 5. The two models used in the study are entirely unrelated and described by different formulations. The $I_{to}$ conductances described by the two models have markedly different activation rates, conductance-voltage relationships, and steady-state inactivation properties. These differences resulted in noticeably different waveforms of dynamic clamp current output when simulated in the same guinea pig ventricular cell (Fig 5 A & C, insets). Nevertheless, the effects of the two $I_{to}$ models on action potential morphology


Copyright Information

and duration were remarkably similar (Fig 5 A & C), so were the shapes of the $I_{to}$ conductance-$APD_{90}$ relationship curves (Fig 5 B & D). Similar experiments were performed in a total of 5 guinea pig cells, and in 3 canine endocardial myocytes (data not shown). These findings argue that to the extent that these models describe a generalized $I_{to}$ conductance, our simulation results are a representation of the true $I_{to}$ functional property.

Guinea pigs have a heart rate over 200 beats per minute. At a higher and more physiological rate, cumulative activation of $I_K$ would favor repolarization of the action potential. We therefore performed simulation studies of $I_{to}$ at pacing rates of 1 and 3 Hz. Simulation of $I_{to}$ at 3 Hz had generally similar effects on guinea pig action potential as observed at 1 Hz (Fig 5E), although a higher density of $I_{to}$ was needed at 3 Hz to achieve all-or-none repolarization (Fig 5F). This shift of the $I_{to}$ density-$APD_{90}$ curve at 3 Hz towards a higher $I_{to}$ density probably reflects a higher degree of cumulative $I_{to}$ inactivation at a higher pacing frequency.

**Effect of sustained outward current on APD**

Our dynamic clamp simulation results in guinea pig ventricular cells differ markedly from those using the gene transfer or cell fusion approaches to introduce Kv4.3 currents in the cells (9,10). In these earlier studies, a sustained outward current was generated in the ventricular cells along with the transient $I_{to}$-like current. A previous computer modeling study suggested that the introduction of such a non-inactivating current contributed to the shortening of the APD by the exogenous Kv4.3 current (6). To test this prediction in real guinea pig ventricular cells, we performed simulations of a


Copyright Information

modified canine epicardial $I_{to}$ model that had a non-inactivating component. Again, simulation of a fully inactivating $I_{to}$ had the typical bi-phasic effect on action potential waveform and duration in guinea pig cells (Fig 6A). In the same cell, simulation of an $I_{to}$ with a 10 to 16% sustained component (a fraction similar to those in Hoppe et al's studies) progressively and significantly suppressed the plateau and shortened the APD over the entire density range we tested (Fig 6B). With the presence of the sustained current, $I_{to}$ density had a monotonic inverse relationship with $APD_{90}$, instead of the bi-phasic relationship when the simulated current fully inactivated (Fig 6C). Similar results were obtained in a total of 4 guinea pig cells. Results shown in figure 6B & C closely reproduced the observations in Hoppe et al's studies, suggesting that the presence of a sustained outward current accounted for the monotonic shortening of APD by $I_{to}$ in these earlier studies.


Copyright Information

## Discussion

Although the action potential waveform in guinea pig ventricular cells shares similarities with those of endocardial ventricular myocytes in large animals such as dog, the underlying ionic current distribution profile in guinea pig and large animals are significantly different. $I_K$ is more prominent in guinea pig ventricular cells than in canine ventricle (15,17), and is balanced by a significantly larger L-type $Ca^{2+}$ current (8,30). Indeed, it was shown that the effect of exogenous Kv4.3 current on action potential in guinea pig ventricular cells (9,10) is distinct to that of $I_{to}$ in canine ventricular cells (27). In the present study, we used the dynamic clamp technique to simulate $I_{to}$ conductances in guinea pig and canine ventricular myocytes, and have shown that, despite the significant differences in cellular electrophysiological background of the two myocytes, the effects of a fully-inactivating $I_{to}$ on the action potential morphology and duration of these two types of myocytes were remarkably similar. Importantly, a distinctive threshold (about 40 pA/pF) existed that separated the effect of $I_{to}$ into two phases. Below this threshold, increasing amounts of simulated $I_{to}$ 1) generated an increasingly deep phase 1 notch, and 2) did not significantly affect the APD at low densities and moderately prolonged the APD at higher densities. $I_{to}$ above the density threshold led to all-or-none repolarization, resulting in spike-like action potentials with dramatically reduced APD. These effects of $I_{to}$ are not linked to the particular mathematical formulations of the $I_{to}$ model, or a specific stimulation rate. Our experimental results are in agreement with the predictions of a modeling study of canine and guinea pig ventricular cells (6), and probably reflect a general role of the $I_{to}$ conductance in regulating the morphology of broad, plateau-possessing cardiac action potentials.


Copyright Information

The underlying mechanism of the bi-phasic APD-$I_{to}$ relationship probably lies in the interplay between $I_{to}$ and the L-type current ($I_{Ca-L}$), as suggested by the modeling study (6). It is clear from our simulation studies that the voltage trajectory at the end of phase 1 repolarization depends on the potential of the notch. $I_{to}$, via its regulation of phase 1 notch potential, either allows reactivation of $I_{Ca-L}$ at the end of phase 1 and the development of the plateau (or the "dome"), or turns off $I_{Ca-L}$ by moving the notch potential below the activation voltage range of $I_{Ca-L}$, and completely suppresses the plateau. Prolongation of the APD occurs when $I_{to}$ causes a delay in the reactivation of $I_{Ca-L}$ and a shift in $I_{Ca-L}$ time course. In our experiments, the average notch potential for such transition between reactivation and deactivation of $I_{Ca-L}$ was around -20 mV for guinea pig ventricular cells, and -24 mV for canine endocardial myocytes.

In our present study, we used perforated-patch clamp recording to preserve physiological intracellular $Ca^{2+}$ handling, and reexamined the effect of $I_{to}$ in canine endocardial cells. Under these conditions, simulation of $I_{to}$ in canine endocardial cells generated action potential waveforms that were remarkably similar to those recorded from canine epicardial tissue or myocyte using microelectrode recordings (13,14,16,18). The APD-$I_{to}$ density relationship is qualitatively similar to our previous findings using whole-cell recordings (Fig 4 of (27)), but with a few noticeable differences. The small depression of APD when $I_{to}$ was around 30 pA/pF was not found in the current study, and was probably an artifact associated with intracellular $Ca^{2+}$ buffering. Instead, progressive APD prolongation was observed over the entire $I_{to}$ density range from ~28 pA/pF to the threshold for all-or-none repolarization. Importantly, in our present study we found that simulation of canine epicardial level of $I_{to}$ (about 20 pA/pF) did not significantly affect


Copyright Information

the endocardial APD, supporting our previous conclusion that physiological levels of $I_{to}$ do not play a significant role in regulating the APD in canine left ventricle. The same, however, cannot be said about $I_{to}$ in canine right ventricular cells. $I_{to}$ density is significantly higher in canine right epicardium than in the left (3,25). Assuming that the APD-$I_{to}$ density relationship shown in figure 4 is shared in right ventricular cells, $I_{to}$ probably moderately prolongs the APD in the right ventricular cells.

$I_{to}$ is conventionally defined in modeling studies as the fully and rapidly inactivating component of the total outward current. Such definition is supported by experimental evidence. It is shown that in mouse ventricular cells, $I_{to}$ inactivates fully and is separate from the non-inactivating outward currents (35). In human atrial and mouse ventricular cells, antisense suppression or functional knockout of the Kv4-generated $I_{to}$ leaves the non-inactivating current intact (1,7,31), arguing that in these native systems, $I_{to}$ and the non-inactivating component are carried by channels with different molecular identifies. For these reason, we defined and modeled $I_{to}$ as a fully-inactivating conductance in our simulation studies. With the simulation of even a small sustained conductance, the bi-phasic APD-$I_{to}$ relationship in guinea pig cells was dramatically changed to a monotonic inverse relationship strikingly similar to those reported earlier (9,10). Simulation of a sustained conductance also eliminated the notch, and suppressed the plateau, closely reproducing Hoppe et al's results. These results point to the importance of the $I_{Kur}$-type sustained current in regulating the action potential morphology. The marked effects of the sustained current are not surprising considering the small net current during the plateau phase. In canine ventricular cells, $I_{to}$ inactivation is rapid and near-complete (Fig 2B). We argued in our earlier study that the large $I_{to}$ size


Copyright Information

in smaller animals such as mouse is responsible for their brief action potentials (27). In addition to a large $I_{to}$, prominent slowly inactivating and non-inactivating currents are present in mouse ventricle (35). These currents, when combined, can make up over half of the total outward current amplitude (35). It is likely that the presence of such slow and sustained currents also contributes importantly to the brief, spike-like action potential in mouse ventricle. In this case, species difference in cardiac action potential morphology is achieved by changes in both channel expression level and function.

Sudden cardiac death, mostly caused by ventricular arrhythmias, is responsible for about half of the mortalities in heart failure patients (20). One of the most characteristic electrophysiological changes in heart failure is the prolongation of the APD, which is believed to predispose the heart to afterdepolarization and reentrant arrhythmias (29). Accompanying the prolongation of APD, down-regulation of $I_{to}$ is consistently observed in heart failure patients as well as animal models (20,28,32). Based on their close correlation, it was proposed that $I_{to}$ down-regulation is an important contributor to APD prolongation in failure (12,32). This is likely to be true in smaller animals, where $I_{to}$ is much beyond the density threshold for all-or-none repolarization (27) and is the major determinant of APD. The same conclusion may not apply to large animals such as humans (22), as the role of $I_{to}$ in regulating action potential morphology differs significantly between small and large animals. $I_{to}$ in canine (27) and human (19) left ventricle is well below the density threshold for all-or-none repolarization, and our APD-$I_{to}$ density curves show that within this density range, reduction of $I_{to}$, regardless of the magnitude, will not prolong the APD under physiological conditions. In heart failure, a concerted change in ion channel expression occurs (33), and the APD-$I_{to}$ density


Copyright Information

relationship reported in our study may be altered as a result of the remodelings of the cellular electrical background. Also, it is possible that downregulation of the Kv4 channel causes a concomitant decrease in the sustained component of the outward current, thereby resulting in APD changes. It would be important to expand our simulation studies to hypertrophy and failure settings.


Copyright Information

## References


1. **Barry DM, Xu H, Schuessler RB and Nerbonne JM**. Functional knockout of the transient outward current, long-QT syndrome, and cardiac remodeling in mice expressing a dominant-negative Kv4 α subunit. *Circ Res* 83:560-567, 1998.
2. **Brunner M, Guo W, Mitchell GF, Buckett PD, Nerbonne JM and Koren G.** Characterization of mice with a combined suppression of Ito and $I_{K,slow}$. *Am J Physiol* 281: H1201-H1209, 2001.
3. **Di Diego JM, Sun ZQ and Antzelevitch C.** Ito and action potential notch are smaller in left vs. right canine ventricular epicardium. *Am J Physiol* 271: H548-H561, 1996.
4. **Findlay I.** Is there an A-type $K^+$ current in guinea pig ventricular myocytes? *Am J Physiol* 284: H598-H604, 2003.
5. **Gima K and Rudy Y.** Ionic current basis of electrocardiographic waveforms: a model study. *Circ Res* 90: 889-896, 2002.
6. **Greenstein JL, Wu R, Po S, Tomaselli GF and Winslow RL.** Role of the calcium-independent transient outward current $I_{to1}$ in shaping action potential morphology and duration. *Circ Res* 87: 1026-1033, 2000.
7. **Guo W, Li H, London B and Nerbonne JM**. Functional consequences of elimination of $I_{to,f}$ and $I_{to,s}$: early afterdepolarizations, atrioventricular block, and ventricular arrhythmias in mice lacking Kv1.4 and expressing a dominant-negative Kv4 α subunit. *Circ Res* 87:73-79, 2000.
8. **Heubach JF, Kohler A, Wettwer E and Ravens U.** T-Type and tetrodotoxin-sensitive $Ca^{2+}$ currents coexist in guinea pig ventricular myocytes and are both blocked by mibefradil. *Circ Res* 86: 628-635, 2000.
9. **Hoppe UC, Johns DC, Marban E and O'Rourke B.** Manipulation of cellular excitability by cell fusion: effects of rapid introduction of transient outward $K^+$ current on the guinea pig action potential. *Circ Res* 84: 964-972, 1999.



Copyright Information

10. **Hoppe UC, Marban E and Johns DC.** Molecular dissection of cardiac repolarization by in vivo Kv4.3 gene transfer. *J Clin Invest* 105: 1077-1084, 2000.

11. **Hund TJ and Rudy Y.** Rate dependence and regulation of action potential and calcium transient in a canine cardiac ventricular cell model. *Circulation* 110: 3168-3174, 2004.

12. **Kaab S, Nuss HB, Chiamvimonvat N, O'Rourke B, Pak PH, Kass DA, Marban E and Tomaselli GF.** Ionic mechanism of action potential prolongation in ventricular myocytes from dogs with pacing-induced heart failure. *Circ Res* 78: 262-273, 1996.

13. **Litovsky SH and Antzelevitch C.** Differences in the electrophysiological response of canine ventricular subendocardium and subepicardium to acetylcholine and isoproterenol. A direct effect of acetylcholine in ventricular myocardium. *Circ Res* 67: 615-627, 1990.

14. **Litovsky SH and Antzelevitch C.** Transient outward current prominent in canine ventricular epicardium but not endocardium. *Circ Res* 62: 116-126, 1988.

15. **Liu DW and Antzelevitch C.** Characteristics of the delayed rectifier current ($I_{Kr}$ and $I_{Ks}$) in canine ventricular epicardial, midmyocardial, and endocardial myocytes. A weaker $I_{Ks}$ contributes to the longer action potential of the M cell. *Circ Res* 76: 351-365, 1995.

16. **Liu DW, Gintant GA and Antzelevitch C.** Ionic bases for electrophysiological distinctions among epicardial, mid-myocardial, and endocardial myocytes from the free wall of the canine left-ventricle. *Circ Res* 72: 671-687, 1993.

17. **Lu Z, Kamiya K, Opthof T, Yasui K and Kodama I.** Density and kinetics of $I_{Kr}$ and $I_{Ks}$ in guinea pig and rabbit ventricular myocytes explain different efficacy of $I_{Ks}$ blockade at high heart rate in guinea pig and rabbit: implications for arrhythmogenesis in humans. *Circulation* 104: 951-956, 2001.

18. **Lukas A and Antzelevitch C.** Differences in the electrophysiological response of canine ventricular epicardium and endocardium to ischemia. Role of the transient outward current. *Circulation* 88: 2903-2915, 1993.


Copyright Information

19. **Nabauer M, Beuckelmann DJ, Uberfuhr P and Steinbeck G.** Regional differences in current density and rate-dependent properties of the transient outward current in subepicardial and subendocardial myocytes of human left ventricle. *Circulation* 93: 168-177, 1996.

20. **Oudit GY, Kassiri Z, Sah R, Ramirez RJ, Zobel C and Backx PH.** The molecular physiology of the cardiac transient outward potassium current ($I_{to}$) in normal and diseased myocardium. *J Mol Cell Cardiol* 33: 851-872, 2001.

21. **Pinto RD, Elson RC, Szucs A, Rabinovich MI, Selverston AI and Abarbanel HD.** Extended dynamic clamp: controlling up to four neurons using a single desktop computer and interface. *J Neurosci Methods* 108: 39-48, 2001.

22. **Priebe L and Beuckelmann DJ.** Simulation study of cellular electric properties in heart failure. *Circ Res* 82: 1206-1223, 1998.

23. **Qin D, Zhang ZH, Caref EB, Boutjdir M, Jain P & el-Sherif N.** Cellular and ionic basis of arrhythmias in postinfarction remodeled ventricular myocardium. *Circ Res* 79: 461-473, 1996.

24. **Ramirez RJ, Nattel S and Courtemanche M.** Mathematical analysis of canine atrial action potentials: rate, regional factors, and electrical remodeling. *Am J Physiol* 279: H1767-H1785, 2000.

25. **Rosati B, Grau F, Rodriguez S, Li H, Nerbonne JM and McKinnon D.** Concordant expression of KChIP2 mRNA, protein and transient outward current throughout the canine ventricle. *J Physiol* 548: 815-822, 2003.

26. **Stengl M, Carmeliet E, Mubagwa K and Flameng W.** Modulation of transient outward current by extracellular protons and $Cd^{2+}$ in rat and human ventricular myocytes. *J Physiol* 511: 827-836, 1998.

27. **Sun X and Wang H-S.** Role of the transient outward current ($I_{to}$) in shaping canine ventricular action potential - a dynamic clamp study. *J Physiol* 564: 411-419, 2005.

28. **Tomaselli GF and Marban E.** Electrophysiological remodeling in hypertrophy and heart failure. *Cardiovasc Res* 42: 270-283, 1999.


Copyright Information

29. **Tomaselli GF, Beuckelmann DJ, Calkins HG, Berger RD, Kessler PD, Lawrence JH, Kass D, Feldman AM and Marban E.** Sudden cardiac death in heart failure. The role of abnormal repolarization. *Circulation* 90: 2534-2539, 1994.

30. **Wang H-S and Cohen IS.** Calcium channel heterogeneity in canine left ventricular myocytes. *J Physiol* 547: 825-833, 2003.

31. **Wang Z, Feng J, Shi H, Pond A, Nerbonne JM and Nattel S**. Potential molecular basis of different physiological properties of the transient outward $K^+$ current in rabbit and human atrial myocytes. *Circ Res* 84:551-561, 1999.

32. **Wickenden AD, Kaprielian R, Kassiri Z, Tsoporis JN, Tsushima R, Fishman GI and Backx PH.** The role of action potential prolongation and altered intracellular calcium handling in the pathogenesis of heart failure. *Cardiovasc Res* 37: 312-323, 1998.

33. **Wickenden AD, Tsushima RG, Losito VA, Kaprielian R and Backx PH.** Effect of $Cd^{2+}$ on Kv4.2 and Kv1.4 expressed in Xenopus oocytes and on the transient outward currents in rat and rabbit ventricular myocytes. *Cell Physiol Biochem* 9: 11-28, 1999.

34. **Winslow RL, Rice J, Jafri S, Marban E and O'Rourke B.** Mechanisms of altered excitation-contraction coupling in canine tachycardia-induced heart failure, II: model studies. *Circ Res* 84: 571-586, 1999.

35. **Xu H, Guo W and Nerbonne JM.** Four kinetically distinct depolarization-activated $K^+$ currents in adult mouse ventricular myocytes. *J Gen Physiol* 113: 661-678, 1999.

36. **Zhabyeyev P, Asai T, Missan S and McDonald TF.** Transient outward current carried by inwardly rectifying $K^+$ channels in guinea pig ventricular myocytes dialyzed with low-$K^+$ solution. *Am J Physiol* 287: C1396-C1403, 2004.


Copyright Information

## Figure Legends

**Figure 1. Mathematical modeling of the canine epicardial $I_{to}$.** A, waveform of the model $I_{to}$ in response to voltage steps ranging from -60 to 50 mV, from a holding voltage of -80 mV. B, peak conductance and time constant of the activation (m) gate of the model $I_{to}$ at various voltages (left), and steady-state and time constant of the inactivation (h) gate at various voltages (right).

**Figure 2. Electrical properties of guinea pig ventricular myocytes.**
A, representative action potential traces recorded from guinea pig ventricular myocyte at 1 Hz and 3 Hz. B, $I_{to}$ is not present in guinea pig ventricular cells, but was readily detectable in canine epicardial cells (inset). Cells were depolarized to voltages ranging from -30 to +50 mV in 10 mV increments, from a holding potential of -70mV at a frequency of 0.1 Hz. Notice the difference in current scales. C, $I_K$ recorded from guinea pig ventricular myocyte at room temperature (24°C). Currents were in response to depolarizing steps ranging from -30 to +50 mV in 10 mV increments, from a holding potential of -40 mV. Tail currents were recorded at -40 mV.

**Figure 3. Dynamic clamp simulation of $I_{to}$ in guinea pig ventricular myocytes.**
A, action potentials recorded at 1 Hz from a guinea pig ventricular myocyte under control conditions (dash line) and with the simulation of a canine epicardial $I_{to}$ (25 pA/pF) using the dynamic clamp (solid line). Bottom trace is the current output of the dynamic clamp. Inset shows the current output on a larger scale. B, action potentials recorded from a


Copyright Information

guinea pig ventricular myocyte with the simulation of incremental densities of $I_{to}$. The "threshold" phenomenon with $I_{to}$ = 48 is shown in the right panel indicated by bold lines. C, action potential duration ($APD_{90}$, expressed as the ratio over control) versus $I_{to}$ density relationships collected from 18 guinea pig ventricular myocytes. The average data are shown in D. Individual traces were aligned such that the last points before all-or-none repolarization fell into one group. Vertical and horizontal error bars are ± S.E.M. of the $APD_{90}$ ratio and $I_{to}$ density, respectively. Asterisks indicate a statistical significance of $P < 0.01$ in a paired Student's *t* test.

**Figure 4. Dynamic clamp simulation of $I_{to}$ in canine endocardial ventricular myocytes.**

A, action potentials recorded from a canine endocardial myocyte with various densities of simulated $I_{to}$. For the left panel, $I_{to}$ density ranged from 5.6 to 33 pA/pF, in increments of about 5.6 pA/pF. B, average $APD_{90}$ ratio vs. $I_{to}$ density relationship for canine endocardial cells. Data are averaged and plotted as described in figure 3 from 7 cells. Asterisks indicate a statistical significance of $P < 0.01$ in a paired Student's *t* test.

**Figure 5. Simulations of different mathematical $I_{to}$ models in guinea pig ventricular cells and at different pacing rates.**

Action potentials recorded from a guinea pig ventricular myocyte with various levels of $I_{to}$ simulated based on canine ventricular $I_{to}$ model (A) and canine atrial $I_{to}$ model (C) (14). The insets show the current output of the dynamic clamp. The $APD_{90}$ ratio vs. $I_{to}$ conductance relationships for A and C are shown in B and D. E, action potential traces


Copyright Information

from a guinea pig ventricular cell with incremental densities of simulated canine epicardial $I_{to}$ at pacing rates of 3 Hz. F, $APD_{90}$ vs. $I_{to}$ density relationships at 1 and 3 Hz for the same cell as in E.

**Figure 6. Effect of a sustained component in $I_{to}$ on action potential shape and duration.**

A, action potentials from a guinea pig ventricular cell with simulation of incremental densities of $I_{to}$ from 8.8 to 60 pA/pF, in increments of ~ 8.8 pA/pF. B, action potentials from the same cell with various densities of simulated $I_{to}$ that had a non-inactivating (sustained) component. Total simulated $I_{to}$ density ranged from 8.9 to 44 pA/pF, in 8.9 pA/pF increments. The sustained component was 16% of the total peak current when elicited by a voltage step to +40 mV from a holding potential of -80 mV. C, $APD_{90}$ ratio vs. $I_{to}$ density relationships from the same cell with simulations of $I_{to}$ that had various fractions of sustained component ($I_s$).


Copyright Information

**Figure 1**

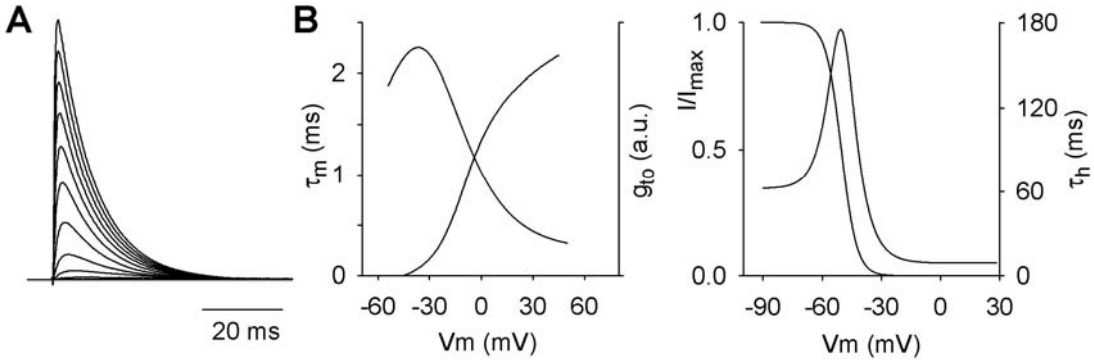



Copyright Information

**Figure 2**

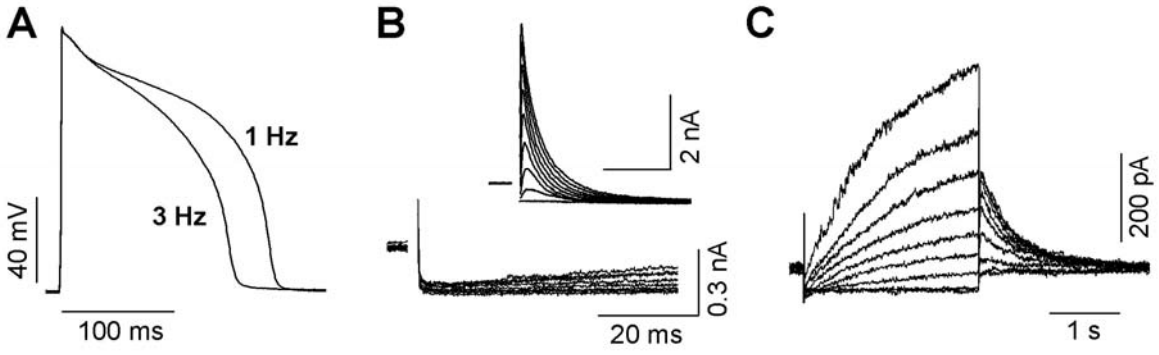



Copyright Information

**Figure 3**

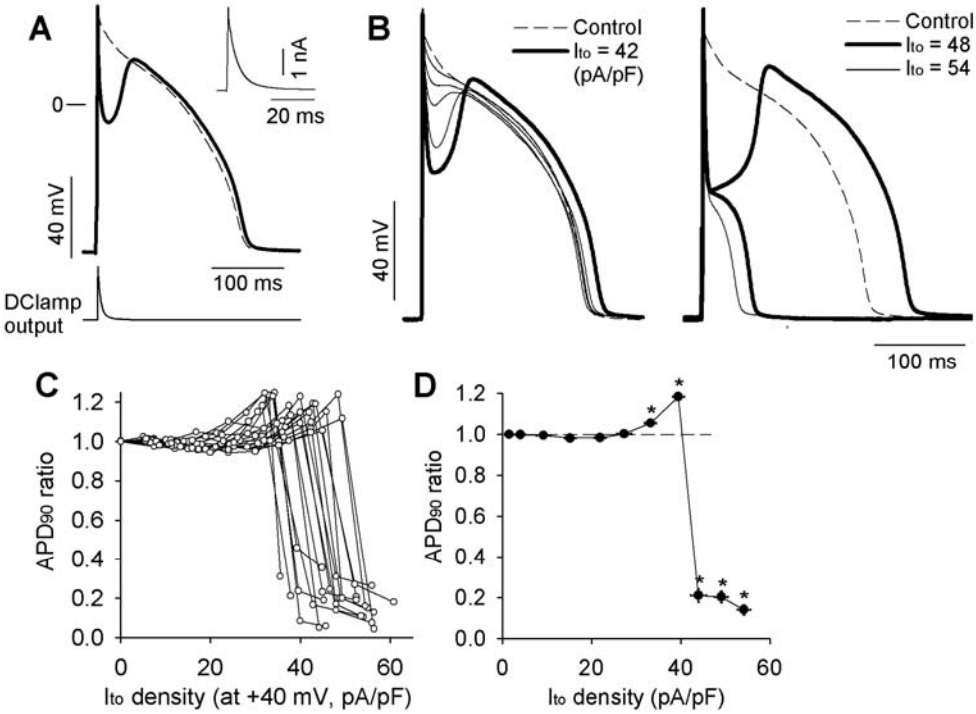



Copyright Information

**Figure 4**

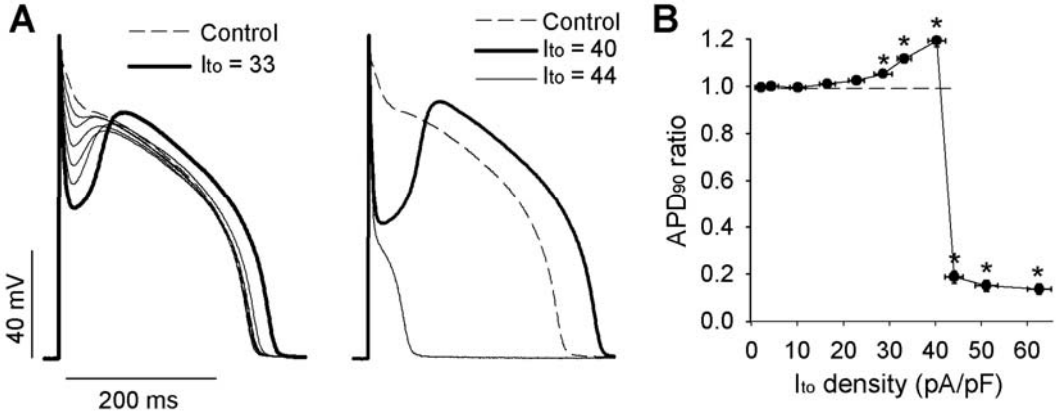



Copyright Information

**Figure 5**

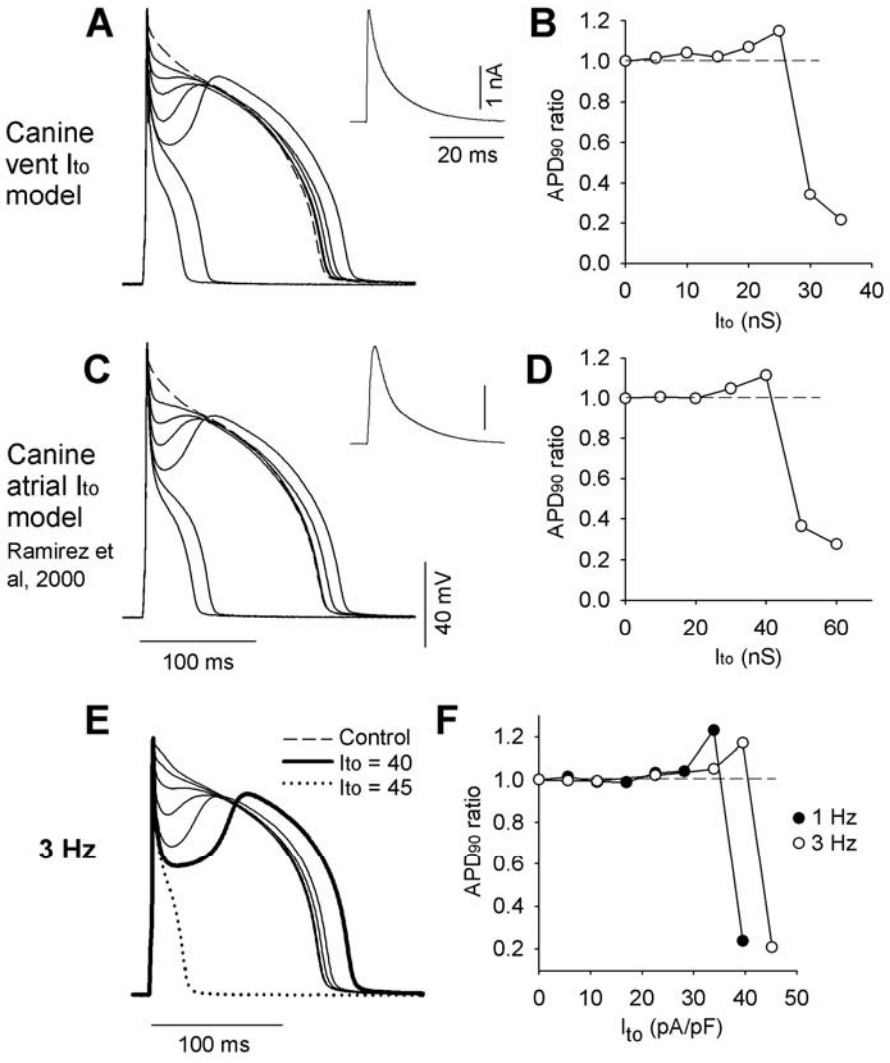



Copyright Information

**Figure 6**

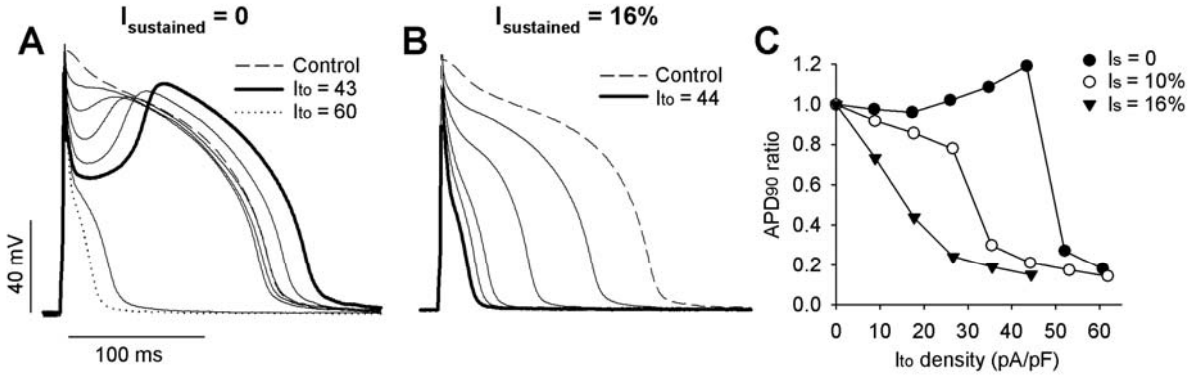



Copyright Information